Aalborg Universitet

Multi-Mode Operation for On-line Uninterruptible Power Supply System

Lu, Jinghang; Savaghebi, Mehdi; Golestan, Saeed; Vasquez, Juan C. ; Guerrero, Josep M.;
Marzabal, Albert

Multi-Mode Operation for On-line Uninterruptible Power Supply System

Jinghang Lu, *Student Member*, *IEEE,* Mehdi Savaghebi, *Senior Member*, *IEEE*, Saeed Golestan, *Senior Member*, *IEEE*, Juan C.Vasquez, *Senior Member*, *IEEE*, Josep M.Guerrero, *Fellow*, *IEEE*, and Albert Marzabal

Abstract—To enhance the robustness and disturbance rejection ability of an on-line uninterruptible power supply (UPS) system, an Internal Model Control (IMC)-based DC-link voltage regulation method is proposed in this paper. Furthermore, the multi-mode operations of the on-line UPS system are investigated and their corresponding control strategies are proposed. The proposed control strategies are capable of achieving the seamless transition in traditional normal mode, PV-aided normal mode, enhanced eco-mode and burn-in test mode. Meanwhile, the uninterruptible load voltage is promised during the mode transition. The small signal analysis is also conducted to investigate the stability of enhanced eco-mode and burn-in test mode. Finally, extensive experimental results are provided to validate the effectiveness of the proposed methods.

Index Terms—Burn-in test Mode; DC-link Voltage; Disturbance Rejection; Enhanced Eco-Mode; Internal Model Control (IMC); PV-aided normal mode; Robustness; Seamless transfer; Uninterruptible Power Supply (UPS);

NOMENCLATURE

Parameter	Description
C	DC-link capacitance[F]
$C_1(s)$	DC-link set-point tracking controller
$C_2(s)$	DC-link proportional controller
D_p	Droop coefficient
D_q	Droop coefficient
E^*	Inverter nominal voltage magnitude [V]
E	Inverter reference voltage magnitude [V]
$F_r(s)$	DC-link disturbance rejection controller
f_s	Sampling frequency of the system
$G_d(s)$	Model difference between Actual and Reference Model
$G_m(s)$	Reference model of DC-link
$G_P(s)$	Actual model of DC-link
$H(s)$	Upper limit of DC-link model uncertainty
I_{DC}	DC-link current
I_{pv}	Current at the terminal of the PV panel [A]
$I_{o\alpha,\beta}$	Output current through Clarke transformation.[A]
k_{pv}	Proportional gain of voltage controller in DC/AC converter
k_{rv}	Resonant gain of voltage controller in DC/AC converter
k_{pi}	Proportional gain of current controller in DC/AC converter
k_{ri}	Resonant gain of current controller in DC/AC converter
k_{pc}	Proportional gain of current controller in AC/DC converter
k_{rc}	Resonant gains of current controller in AC/DC converter
P	Instantaneous active power of the UPS system
P_{DC}	The injected DC-link active power [W]
P_{ext}	External power that flows out of DC link [W]
P_t	Rectifier AC-side terminal power [W]
P_s	Grid side active power [W]
P_{s_ref}	Reference active powers [W]
P_{LPF}	Active power through a low-pass filter
Q	Instantaneous reactive power of the UPS system
Q_{LPF}	Reactive power through a low-pass filter
R_p	Equivalent resistance of total switching loss [Ω]
R_v	Virtual resistance in the control of DC/AC converter [Ω]
V_{DC}	DC-link voltage [V]
$V_{c\alpha,c\beta}$	Output voltage through Clarke transformation.
V_{pv}	Voltage at the terminal of the PV panel [V]
λ_1	Tuning parameter of $C_1(s)$
λ_2	Tuning parameter of $F_r(s)$
ω^*	Inverter nominal frequency [rad/s]
ω	Inverter reference frequency [rad/s]
ω_{syc}	Synchronization frequency [rad/s]
τ	Time constant of the low-pass filter.
φ	Power angle

I. INTRODUCTION

With the increasing infrastructure of data center, communication network, and IT servers, Uninterruptible Power Supply (UPS) systems have been widely equipped in recent years [1, 2]. According to the IEC Standard 62040-3 [3], the UPS systems are categorized as on-line, off-line, and line-interactive UPSs in the normal mode of operation. The on-line UPS system is commonly installed as it isolates the load from the grid that may suffer from frequency variation and voltage irregularity. An on-line UPS system usually consists of a rectifier, one or more inverters, a battery bank with its associated DC/DC converter, Transient Voltage Surge Suppressor (TVSS), and a static bypass switch [4]. A multi-inverter configuration of the on-line UPS is employed for applications where a higher reliability and more redundancy are

Jinghang Lu, Mehdi Savaghebi, Saeed Golestan, Juan C.Vasquez, and Josep M.Guerrero are with the Department of Energy Technology, Aalborg University, Aalborg DK-9220, Denmark. (email:jgl@et.aau.dk, mes@et.aau.dk, ygu@et.aau.dk, sgd@et.aau.dk, juq@et.aau.dk, joz@et.aau.dk)
Albert Marzabal is with Salicru, Barcelona, Spain. (email: Albert.Marzabal@salicru.com)

required (see Fig. 1) [5].

In the Traditional Normal Mode (TNM) operation of an on-line UPS system, the load power is provided by the combination of AC/DC rectifier and DC/AC inverter. Recently, several studies have been conducted by integrating fuel cell or multiple energy sources into the UPS system [6-9], which claims to improve the performance under both normal mode and backup mode of operation. Among these studies, [9] proposed a seamless transfer control strategy for the fuel cell-based UPS system. [6-8] proposed a Super UPS topology, where the fuel cell, Photovoltaic (PV) generation, and gas engine are all integrated into the UPS system. However, incorporating all these energy units into the UPS system inevitably increases the client's economic burden and furthermore, energy management of such a system is quite complicated and challenging. In addition, considering the slow dynamics of the fuel cell and high cost of gas pipeline construction, only integrating the PV unit into the UPS system may be a promising solution, as the implementation of PV energy helps to reduce the cost of the electricity from the grid and it is an eco-friendly generation system. Therefore, the PV-aided Normal Mode (PNM) of on-line UPS system can improve the overall system performance considering economic and environmental benefits.
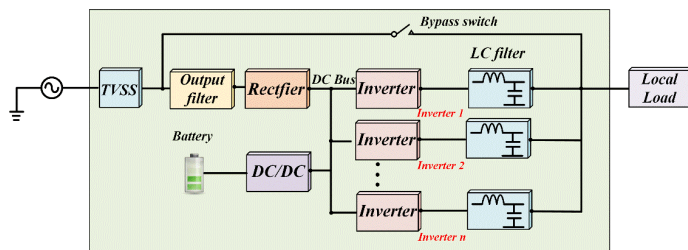

Fig.1. Diagram of the on-line UPS system with multiple inverters

However, if the PV system is unavailable, i.e., during the night, the operation of the on-line UPS system has to return to the TNM. To save more energy, the Eco-mode operation in the UPS system has recently been proposed by several UPS manufacturers [10, 11]. The Eco-mode is similar to the normal operation in the off-line UPS system, where the load is directly fed from the grid through the bypass switch, and the inverters operates in "standby" mode as shown in Fig. 2. Notice that the protection device (TVSS) is located between the bypass switch and the grid. Hence, during the Eco-mode operation, the surge voltage and current have no effect on the local load. This mode shows the benefits that the efficiency of the power delivery is typically between 98% to 99%, compared to 93%-96% of TNM operation [10]. Nonetheless, usually, UPS system provides both active and reactive power to the load. If the UPS is operated in this Eco-mode, the utility typically charges extra fees for delivering the reactive power to the load. Therefore, Active Eco-Mode (AEM) or Improved Eco-Mode (IEM) concept is proposed by the UPS manufacturers [10, 11], which shows that the active power of the load is directly provided by the grid while its reactive power is supplied by the inverter of the UPS system. For example, in [12], an AEM through the current control of inverter is proposed. Since the voltage control strategy is implemented for TNM, the load voltage may suffer

from significant fluctuations during control strategy switch, and the smooth transition is greatly affected between TNM and AEM. Therefore, an Enhanced Eco-mode (EEM) control strategy is investigated in this paper. The proposed EEM operation guarantees the inverters are always controlled in Voltage Control Mode (VCM) both in the TNM and the EEM operation. In this way, the seamless transition between TNM and EEM is promised, and, therefore, the output voltage is not affected during the transition.
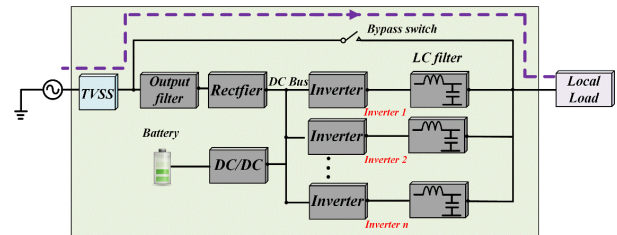

Fig.2 Traditional Eco-mode of on-line UPS system

In addition, a new UPS system needs to do the burn-in test for the quality certification. Traditionally, in the Burn-in Test Mode (BTM), the output of the UPS system is connected to a resistor bank. This causes an increased energy consumption and, therefore, an additional cost for the final product. Therefore, the energy saving methods are considered to be important for both UPS manufacturers and the utility. Until now, some energy saving methods in the BTM have been proposed in [13-15]. [14] proposed a BTM method by placing an inductor and a transformer between the output of the UPS system and the grid. However, the bulky and heavy transformer is quite inconvenient for the burn-in test. To overcome this drawback, current controlled inverter [13] and open-loop voltage controlled inverters [15] have been suggested to replace the passive equipment. However, these control strategies are either too complicated or trigger the harmonics propagation. Moreover, VCM is usually adopted in the TNM, the same control mode (VCM) is thus desirable to achieve the BTM . Consequently, by applying the same control mode in both the TNM and the BTM, the seamless transition could be realized and the cost for the wasted energy could be saved.

Finally, from the discussion as mentioned above, it is noticed that all these operation modes (TNM, PNM, EEM, BTM) involve the DC-link voltage control. The robust and efficient control of the DC-link voltage is highly important, as this link plays a key role in the energy transfer from the utility to the DC-link and further delivering to the critical load. If the DC-link voltage is not controlled appropriately, the disturbance caused by connecting/disconnecting load may trigger the DC-link voltage protection and affect the stable operation of the UPS system. In the on-line UPS system, the DC-link voltage is regulated by the AC/DC converter, where a dual-loop control structure is implemented [16]. The proportional-integral (PI) controller is implemented for the outer loop control to maintain a constant DC-link voltage. Meanwhile, the synchronous reference frame PI controllers or the stationary reference frame proportional-resonant (PR) regulators are adopted for the inner

loop current tracking [17]. In order to enhance the DC-link voltage dynamics in the presence of disturbances, a feedforward control is added in the voltage control loop by measuring the external power [18]. This method, however, requires additional sensors, which may not be desirable from the reliability and cost points of view [19-21]. This is particularly true for the UPS systems where the "plug and play" function needs to be realized by expanding more UPS modules according to the client's requirement [22, 23]. Therefore, a DC-link voltage control with sensor-less control strategy needs to be investigated.

Recently, several observer-based methods have been proposed to improve the dynamics of the DC-link voltage with a sensor-less control strategy [24-26]. In [25]-[26], nonlinear disturbance observer-based control strategies are implemented for DC-link voltage control. However, these methods are highly nonlinear and, therefore, difficult to analyze and design. In [24], an enhanced state observer (ESO) based DC-link voltage control is suggested and offers robust performance and high disturbance rejection ability. However, this method highly depends on the observer's bandwidth. In addition, notice that all the aforementioned methods are designed in time-domain, the frequency domain design methods, which are more familiar to the engineers, have not been investigated. The internal model control (IMC) method, designed in the frequency domain, has shown good reference tracking, disturbance rejection, and robustness against the parameter variation. This method has been successfully applied in motor control, PV system, and DC/DC converters [27-29], but to the best of the author's knowledge, has not been applied in the DC-link voltage control. So, in this paper, the IMC-based control strategy will be investigated for the DC-link voltage regulation.

proposed. Based on the proposed control strategies for multi-mode operation, the on-line UPS system can easily shift its operation modes by changing the desired active and reactive power reference according to the requirement. The seamless transition among different operation modes are also realized and the uninterruptible load voltage is promised during the mode transition. Furthermore, the small signal analysis is conducted to investigate the stability of EMM and BTM. Finally, extensive experimental results are provided to validate the effectiveness of the proposed methods.

The rest of the paper is arranged as follows: Section II describes the proposed IMC-based DC-link voltage control strategy for the on-line UPS system. Section III explained the control strategies of multi-mode operation in the on-line UPS system, the small signal analysis is also given in this section. The extensive experimental results are provided to show the effectiveness of the proposed methods in Section IV. Finally, the conclusions are given in Section V.

II. IMC-BASED DC-LINK VOLTAGE CONTROL STRATEGY

Fig. 3 shows the system diagram of the on-line UPS system in this paper, where it consists of the PV panel, the battery, a rectifier, several inverters, the TVSS, and DC/DC converters. In this diagram, the boost-type and bi-directional DC/DC converters are responsible for the PV and the battery's power delivery, respectively. A three-phase PWM full bridge converter with an L-type filter is used for the power supply from the grid to the DC link. The paralleled inverters achieve the plug 'n' play control with the VCM and power the load up. In addition, bypass switch is closed when the UPS system shifts its operating mode from the TNM to the EEM or the BTM while
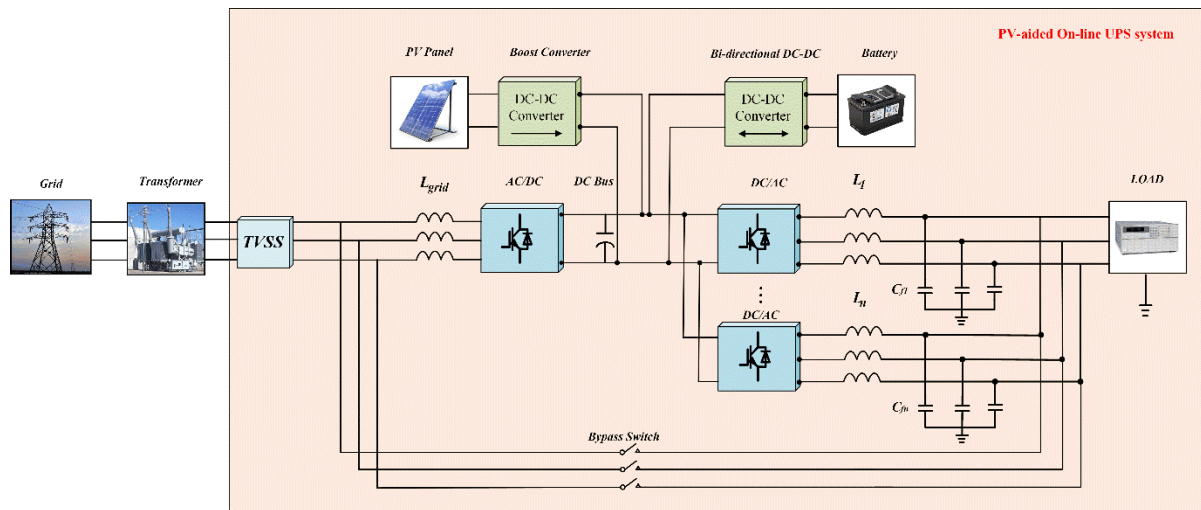

Fig.3. The diagram of the on-line UPS system

In this paper, first, the standard IMC-based control strategy is derived for the sensor-less regulation of the DC-link voltage of the on-line UPS system. Then, a two-port IMC method is proposed for the DC-link voltage control, which results in an enhanced tracking and disturbance rejection ability. In addition, the multi-mode operation for the on-line UPS system is investigated and their corresponding control strategies are

TVSS promises the surge voltage and current do not affect the UPS stable operation during these modes.

The schematic diagram of the AC/DC converter with its associated control strategy for the on-line UPS system is shown in Fig. 4. The control diagram consists of cascaded control loops: the outer DC-link voltage control loop, which is designed in this section, and inner current control loop. Note that the

general load in Fig. 4 represents the PV, battery, and the inverter units. As is shown in Fig. 4, the AC/DC converter is responsible for regulating the DC-link voltage. Therefore, a robust control strategy of DC-link voltage is quite important for the stable operation of UPS system. In the following parts of this section, the proposed two-port IMC-based DC-link controller will be illustrated.
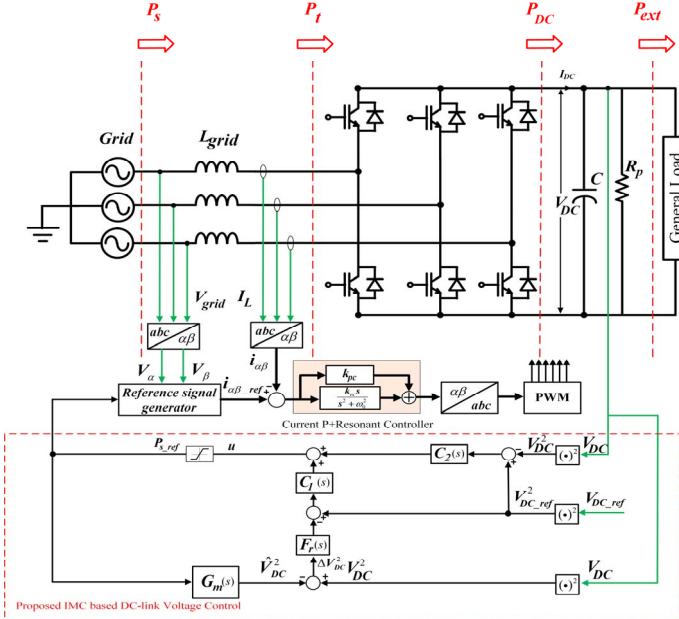

Fig.4. Schematic diagram of the AC/DC converter with the proposed two-port IMC-based DC-link voltage control in PV-aided UPS system

A. DC-Link Modeling

In the on-line UPS system, the DC-link voltage, which is regulated by the AC/DC rectifier, keeps constant by balancing the injected and the output active power of the DC link. Therefore, the power balance across the DC link (see Fig.4) is expressed as :

$$\frac{d}{dt}(0.5CV_{DC}^2) = P_{DC} - P_{ext} - \frac{V_{DC}^2}{R_p} = P_t - P_{ext} - \frac{V_{DC}^2}{R_p} \quad (1)$$

where V_{DC} is the DC-link voltage, and C is the DC-link capacitance. The injected active power P_{DC}, which is equal to the rectifier AC-side terminal power P_t, is expressed as: $P_{DC} = V_{DC}I_{DC}$. P_{ext} is the external power that flows out of the DC-link capacitor. R_p represents the total switching loss in the converter circuit. If the instantaneous power of AC-side filter is not considered, the AC-side terminal power P_t is equal to the AC-side power P_s. A DC-link voltage model is thus derived and is independent of the operating point:

$$\frac{d}{dt}(0.5CV_{DC}^2) = P_s - P_{ext} - \frac{V_{DC}^2}{R_p} \quad (2)$$

where V_{DC}^2 and P_s are the output and control input, respectively. Notice that P_{ext} acts like a disturbance here. Taking the Laplace transform of both sides of (2) results in:

$$V_{DC}^2(s) = \frac{2R_p}{CR_ps+2}P_s(s) - \frac{2R_p}{CR_ps+2}P_{ext}(s) \quad (3)$$

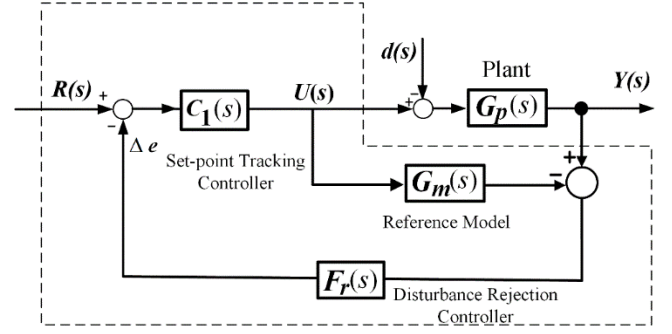*B. Two Degree of Freedom (2-DOF) IMC-Based DC-link Voltage Controller Design*

Fig.5. The 2-DOF internal model controller structure

From the discussion of section A, it is found that the DC link may suffer from external disturbance, such as: DC link current change caused by the connection/disconnection of the load, and internal disturbance, such as system parameter variation. However, the traditional method such as PI control, may not deal with this disturbance effectively. As the two-degree (2-DOF) IMC-based controller can achieve good performance in the external disturbance rejection and internal system parameter variation without measuring DC-link external power P_{ext}, this control strategy will be applied in the DC link voltage regulation.

Fig. 5 shows the structure of a 2-DOF IMC-based controller in the Laplace domain. In Fig. 5, $G_P(s)$ is the actual plant, $G_m(s)$ is the reference model and also named as the internal model, $C_1(s)$ and $F_r(s)$ are the set-point tracking controller and the disturbance rejection controller, respectively.

When the 2-DOF IMC-based strategy is applied to the DC-link voltage controller, the control diagram is shown in Fig. 6. The control structure includes an inner current loop for controlling the rectifier output current and an outer voltage loop for regulating the DC-link voltage. To avoid a dynamic interaction between the inner and the outer loops, the bandwidth of the former one is often considered to be much larger than that of the latter one. It implies that, during the DC-link controller design, the dynamics of the current regulation loop can be neglected and assume that $P_s \cong P_{s\_ref}$, where P_{s_ref} and P_s are the reference and output active powers, respectively (see Fig. 6).

From Fig. 6, the closed-loop transfer function for the DC-link voltage is expressed as:

$$V_{DC}^2 = \frac{C_1(s)G_P(s)}{1+C_1(s)F_r(s)[G_P(s)-G_m(s)]}V_{DC\_ref}^2 - \frac{G_P(s)[1-C_1(s)F_r(s)G_m(s)]}{1+C_1(s)F_r(s)[G_P(s)-G_m(s)]}P_{ext} \quad (4)$$

where V_{DC_ref} is the DC-link reference voltage, V_{DC} is the regulated DC-link voltage, P_{ext} is the external active power and considered as the disturbance. $G_p = \frac{2R_p}{CR_ps+2}$, G_m is the designed reference model, and G_d indicates uncertainty. The relationship between G_p and G_m is expressed as:

$$G_p = G_m + G_d \quad (5)$$

The purpose of the IMC-based control strategy, by designing the controller $C_1(s)$ and $F_r(s)$, is achieving a robust tracking

and high disturbance rejection ability in the presence of a considerable the uncertainty in the model. According to [27, 30, 31], the set-point tracking controller $C_1(s)$ is designed as $C_1(s) = \frac{1}{\lambda_1 s+1} G_m^{-1}(s)$ and thus, promises the robust and fast tracking ability. Note that λ_1 is the tuning parameter of $C_1(s)$. Meanwhile, the disturbance rejection controller $F_r(s)$ is designed as z. Note as well that λ_2 is the tuning parameter of $F_r(s)$.

If the reference model is equal with actual plant, i.e., $G_p(s) = G_m(s)$, from (4) and (5), the closed-loop transfer function for the DC-link voltage is expressed as:

$$V_{DC}^2 = \frac{1}{\lambda_1 s+1} V_{DC\_ref}^2 - \frac{2R_p(\lambda_1\lambda_2 s^2+(\lambda_1+\lambda_2)s)}{(CR_p s+2)(\lambda_1 s+1)(\lambda_2 s+1)} P_{ext} \quad (6)$$

As the DC-link voltage is controlled at the frequency $s = j\omega = 0$, by substituting $s = 0$ into (6), we have the expression:

$$V_{DC}^2 = V_{DC\_ref}^2 \quad (7)$$

Eq. (7) shows that at the steady-state, the 2-DOF IMC control strategy is able to track the reference with zero-steady state error. In addition, the error of the feedback signal $E(s)$ is expressed as:

$$E(s) = \frac{1}{C_1(s)F_r(s)(G_P(s)-G_m(s))+1} V_{DC\_ref}^2 + \frac{F_r(s)G_P(s)}{C_1(s)F_r(s)(G_P(s)-G_m(s))+1} P_{ext} \quad (8)$$

When there is the difference between the plant $G_P(s)$ and the reference model $G_m(s)$, $E(s)$ provides the information of the disturbance and the plant mismatch. The robustness can be obtained by compensating for the deviation appropriately.

In this paper, the actual plant is expressed as: $G_p = \frac{2R_p}{CR_p s+2}$ and the reference model is expressed as: $G_m = \frac{2}{Cs}$, as the R_p is considered as the uncertainty in the system.

The parameter λ_1 of $C_1(s)$ mainly decides the DC-link voltage closed-loop bandwidth. In our system, the DC link closed-loop bandwidth is chosen to be 20rad/s, hence, $\lambda_1 = 1/20$. In addition, the parameter λ_2 of $F_r(s)$ is usually chosen to be much smaller than λ_1 to make sure disturbance rejection

controller's bandwidth is large enough to detect/reject disturbance. but too large bandwidth may interact with current controller's bandwidth, and, as a result, may cause stability issue due to the coupling. Moreover, too large bandwidth may bring the noise as well, Considering the above requirement, $\lambda_2 = 1/200$.[31-34].

C. Stability Analysis

In this section, the small gain theorem is applied to ensure the stability of the system uncertainty. The necessary and sufficient condition for the stable system is expressed as :

$$|C_1(s)F_r(s)|H(s) < 1 \quad (9)$$

where $H(s)$ is the upper limit ($H(s) > \Delta G_d$), if the model mismatch exists, the model error is expressed as:

$$G_d(s) = G_p(s) - G_m(s) \quad (10)$$

So, when $s = 0$, $F_r(0) = 1$. By substituting it into (9), the following equation can be obtained:

$$|C_1(0)|H(0) < 1 \quad (11)$$

By substituting $C_1(s) = \frac{1}{\lambda_1 s+1} G_m^{-1}(s)$ and $G_d(s) = G_p(s) - G_m(s)$ into (11) and making some arrangement, the stability requirement can be obtained:

$$|G_m^{-1}(0)G_p(0) - 1| < 1 \quad (12)$$

From (12), it is seen that system is stable under the condition that uncertainty value is no more than two times the plant.
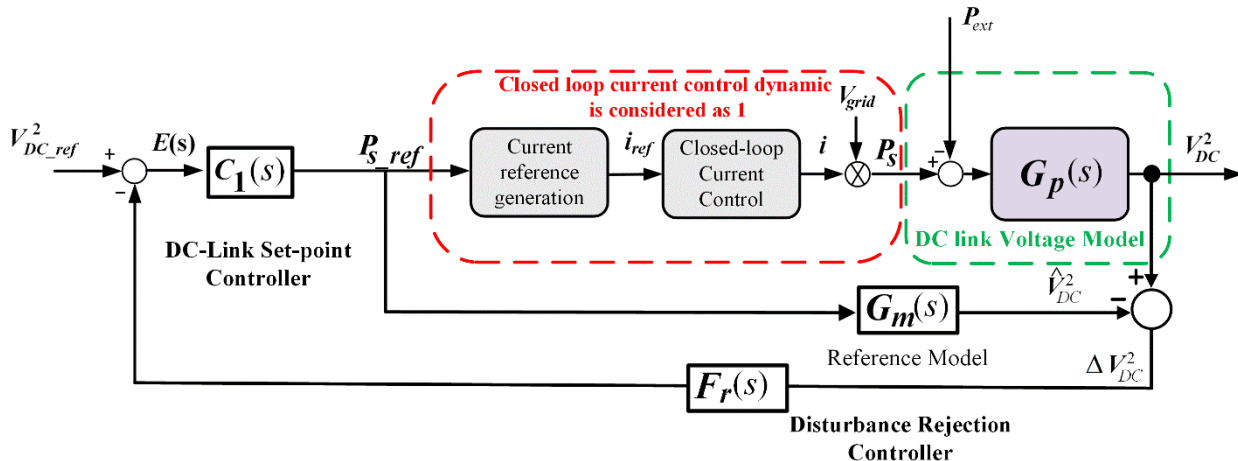

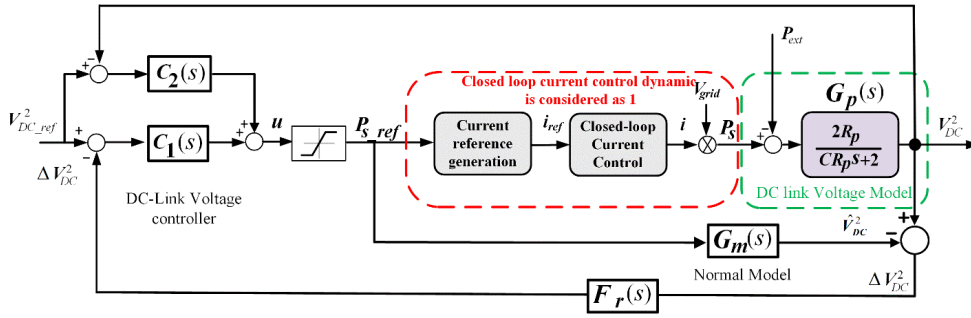Fig.6. The 2-DOF internal model controller structure.

Fig.7. Block diagram of the modified IMC method for DC-link voltage control

D. Two-Port IMC-Based DC-link Voltage Controller Design

In order to enhance the tracking and disturbance rejection ability, a feedback control block $C_2(s)$ is added in the 2-DOF IMC-based DC-link voltage control diagram by using the two-port IMC structure [34, 35], as shown in Fig. 7. Note that active power reference P_{s_ref} is limited in practice and the relationship between the input u and P_{ref} is expressed as:

$$P_{ref} = \begin{cases} u & |u| \leq P_{ref\_max} \\ P_{ref\_max} \cdot sign(u) & |u| > P_{ref\_max} \end{cases} \quad (13)$$

where P_{ref_max} is the maximum active power reference. The controller of $C_2(s)$ is designed as a proportional term, which is expressed as:

$$C_2(s) = k_p \quad (14)$$

To simplify the analysis of the two-port IMC based DC-link control strategy, the saturation block is neglected by assuming: $P_{ref} = u$. From Fig.7, the closed-loop expression for V_{DC}^2 is expressed as:

$$V_{DC}^2 = \frac{[C_1(s)+C_2(s)]G_P(s)}{1+C_1(s)F_r(s)[G_P(s)-G_m(s)]+C_2(s)G_P(s)} V_{DC\_ref}^2 - \frac{G_P(s)[1-C_1(s)F_r(s)G_m(s)]}{1+C_1(s)F_r(s)[G_P(s)-G_m(s)]+C_2(s)G_P(s)} P_{ext}$$
$$(15)$$

If the internal mode is accurate, i.e. $G_P(s) = G_m(s)$, from (15), the closed-loop transfer function for the DC-link voltage is expressed as:

$$V_{DC}^2 = \frac{CR_p s+k_p \lambda_1 s+2+2R_p k_p}{(CR_p s+2+2R_p k_p)(\lambda_1 s+1)} V_{DC\_ref}^2 - \frac{2R_p(\lambda_1 \lambda_2 s^2+(\lambda_1+\lambda_2)s)}{(CR_p s+2+2R_p k_p)(\lambda_1 s+1)(\lambda_2 s+1)} P_{ext}$$
$$(16)$$

By comparing (16) with (6), it is observed that the parameter k_p of controller $C_2(s)$ can be tuned properly to reduce the recovery time in the presence of the load disturbance, i.e., $\frac{CR_p}{2+2R_p k_p} < \frac{CR_p}{2}$.

It should be noted the parameter selection of $C_2(s)$ should keep the poles of closed loop transfer function in Eq.(15) are all located in the left half plane. In addition, the system stability is not affected by the saturation block, according to [36],if the controller is a proper transfer function with minimum phase, the stability will not be affected by the saturation block. In our system, the controller $C_1(s)$ satisfies the above requirement. But the DC link voltage control transient dynamic performance may be affected by the saturation block, which is called windup.

However, the controller $C_2(s)$ of two port IMC based control strategy can compensate for the effect of saturation as anti-windup to improve the tracking performance. [34, 37].

E. Inner loop Current Controller Design

In this AC/DC converter, the proportional-resonant controller is adopted for the inner loop current control, which is expressed as:

$$G_k(s) = k_{pc} + \frac{k_{rc}s}{(s^2+\omega_1^2)} \quad (17)$$

where k_{pc} and k_{rc} are the proportional and resonant gains of the current controller, ω_1 is the grid fundamental angular frequency. For the parameter selection, two useful equations (18) and (20) can quickly help select the appropriate parameter [38], the proportional gain parameter is calculated as:

$$k_{pc} = \alpha_c L \quad (18)$$

where α_c is the desired current controller closed-loop bandwidth. L is the inductance value of the AC/DC converter. α_c should be selected to be:

$$\alpha_c \leq \frac{\omega_s}{10} \quad (19)$$

where ω_s is the angular sampling frequency, which is expressed as: $\omega_s = \frac{2\pi}{T_s} = 2\pi f_s$, f_s is the sampling frequency of the system. Finally, according to the system parameter listed in Table I, $k_{pc} = 7$.

The selection of resonant gain k_{rc} can be calculated by the suggested formula :

$$k_{rc} = 2\alpha_1 \alpha_c L = 2\alpha_1 k_{pc} \quad (20)$$

where $\alpha_1 \ll \alpha_c$, in addition, according to the suggestion in [38] $\alpha_1 < \omega_1$. In the system, α_1 is selected as $\alpha_1 = 30$, so, $k_{rc} = 2*30*7 = 420$

III. CONTROL STRATEGIES FOR MULTI-MODE OPERATION IN THE ON-LINE UPS SYSTEM

As previously stated in the Introduction section, when the grid is normal, the operation mode is categorized as TNM, PNM, EEM and BTM (see Fig. 8). On the other hand, these modes need to switch to the back-up mode when a grid fault occurs. Since this paper mainly focuses on the control strategies and their seamless transition between different operating modes when the grid is normal, the discussion about the transition between the grid normal operating modes and the back-up mode

is out of scope of this paper. In the following parts of this section, the details of the control strategy for these modes will be discussed.
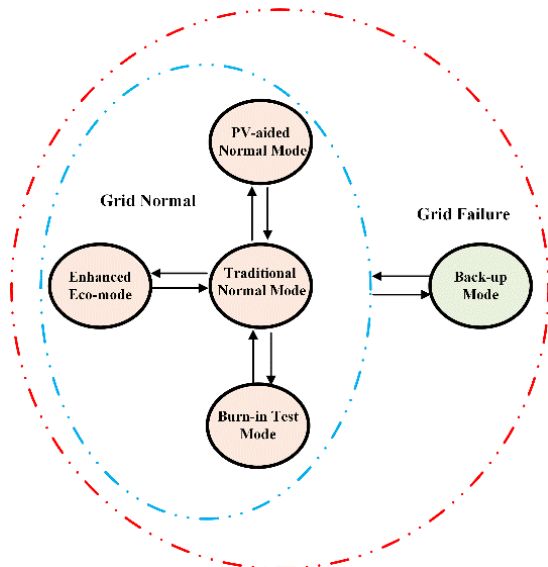

Fig.8. Operating modes of the on-line UPS system

A. PV-Aided Normal Mode of Operation

In the TNM operation of the on-line UPS system, the load power is provided by the grid though the AC/DC rectifier and the DC/AC inverters. When the small rating PV system is integrated into the on-line UPS system, the load active power is supplied by the combination of the PV system and the grid, as shown in Fig.9. Note that the battery has been fully charged and operated in standby mode, which means the battery does not involve the power supply to the load in the normal mode. The PV panel should always be working in Maximum Power Point Tracking (MPPT) mode to save the electricity from the grid.
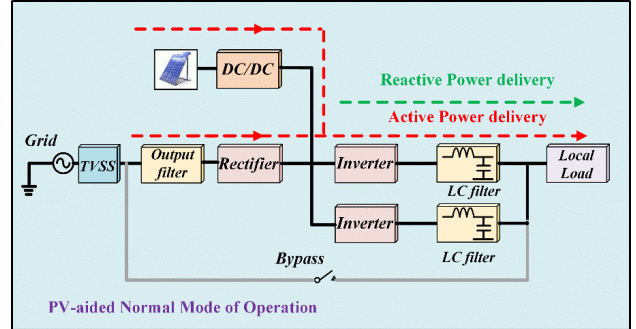
Fig.9. Power flow in the PNM of the on-line UPS system.

1) Control Strategy for DC/AC Inverters in on-line UPS System

Fig. 10 shows the control strategy of the UPS system in the PNM operation. The droop control strategy is implemented for the parallel-connected the inverter modules. Due to the short distance from the inverter to the load in the UPS system, the line impedance is considerably small. And a virtual resistance R_v is embedded in the control diagram to increase the system

Fig.10. The control strategy of the PNM in on-line UPS system.

stability. As the output impedance shows a resistive nature by adding the virtual resistance, $Q{\sim}\omega$ and $P{\sim}E$ droop control strategy is implemented in the control loop [39] and expressed as :

$$\omega = \omega^* + D_q Q_{LPF} \tag{21}$$
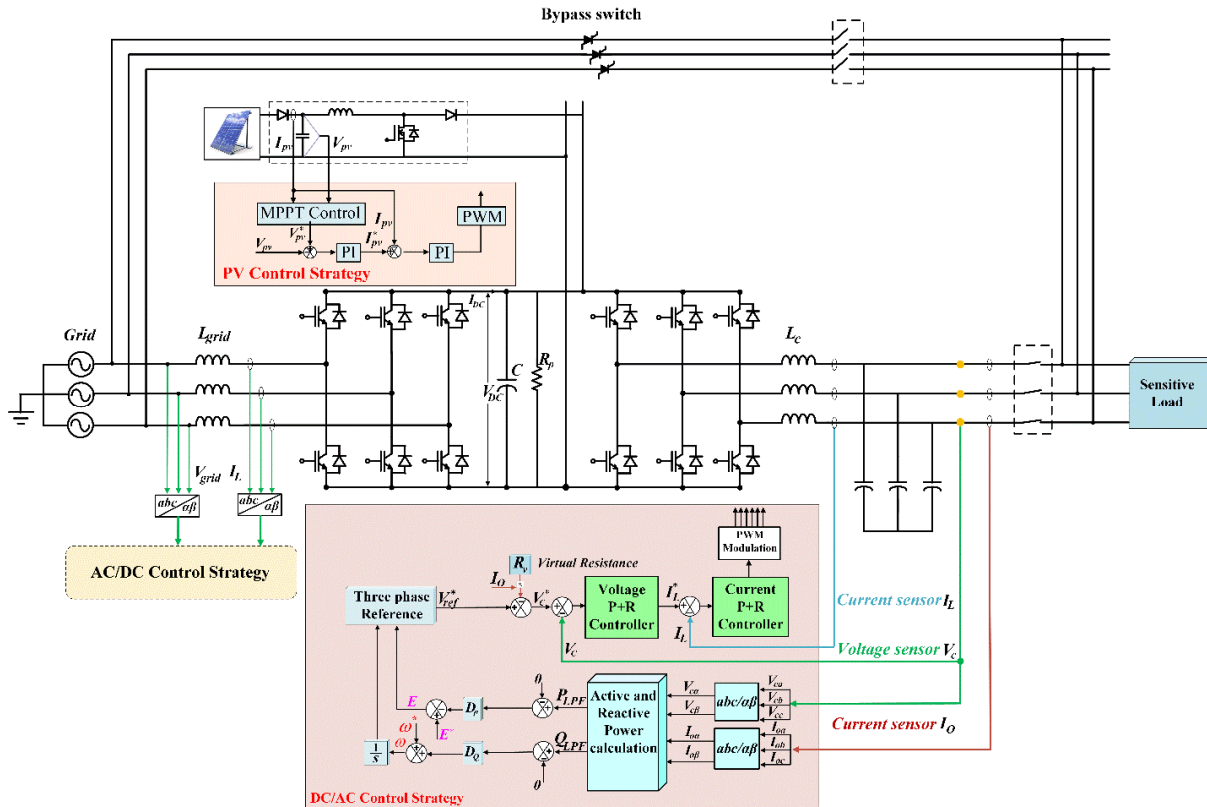
$$E = E^* - D_p P_{LPF} \tag{22}$$

where ω^* and ω are the inverter nominal and reference frequency. E^* and E are the inverter nominal and reference voltage magnitude. D_p and D_q are the droop coefficients for the controlling the output active power P_{LPF} and reactive power Q_{LPF} through a low-pass filter, respectively. The calculated active power P_{LPF} and reactive power Q_{LPF} are expressed as:

$$P_{LPF} = \frac{3}{2(\tau s+1)}(V_{c\alpha}I_{o\alpha} + V_{c\beta}I_{o\beta}) \tag{23}$$

$$Q_{LPF} = \frac{3}{2(\tau s+1)}(V_{c\beta}I_{o\alpha} - V_{c\alpha}I_{o\beta}) \tag{24}$$

where τ is the time constant of the low-pass filter. $V_{c\alpha}$ and $V_{c\beta}$ are the output voltage through Clarke transformation. $I_{o\alpha}$ and $I_{o\beta}$ are the output current through Clarke transformation.

In addition, in order to achieve excellent reference tracking in the output voltage and limit the inductor's current during the transients as a protection feature, a dual-loop strategy with outer voltage proportional resonant (P+R) control and inner current proportional resonant (P+R) control strategy is adopted in the paper. These two controller are expressed as:

$$G_v(s) = k_{pv} + \frac{k_{rV}s}{s^2+(\omega_o)^2} + \sum_{h=5,7}\frac{k_{vh}s}{s^2+(h\omega_o)^2} \tag{25}$$

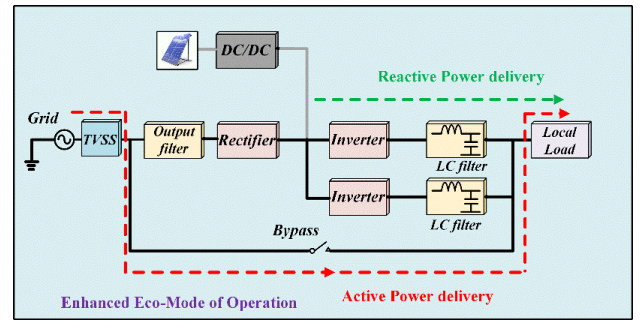$$G_i(s) = k_{pi} + \frac{k_{ri}s}{s^2+(\omega)^2} \tag{26}$$

Fig.11. Power flow in the EEM of the on-line UPS system.

where k_{pv} and k_{pi} are the proportional terms, k_{rV} and k_{ri} are the resonant term coefficient at ω. k_{vh} is the resonant coefficient term for the hth harmonics (h=5th, 7th). The inner current loop is designed to provide a sufficient damping and protect the inductor's current from an overcurrent. Finally, it should be noted that if the nonlinear load is connected as the sensitive loads, the harmonic compensator should be added in the voltage controller of DC/AC converter to enhance the harmonic rejection ability of the output voltage[23]. Note that the control strategy for the rectifier has been shown in Fig. 4 and is not reiterated in this section.

2) PV System and the Control Diagram

The PV panel is operated in the MPPT as shown in Fig. 10, where the power of the PV panel is expressed as:

$$P_{pv} = V_{pv}I_{pv} \tag{27}$$

Where V_{pv} and I_{pv} are the voltage and current at the terminal of the PV panel. Several MPPT algorithms, such as: Perturb &

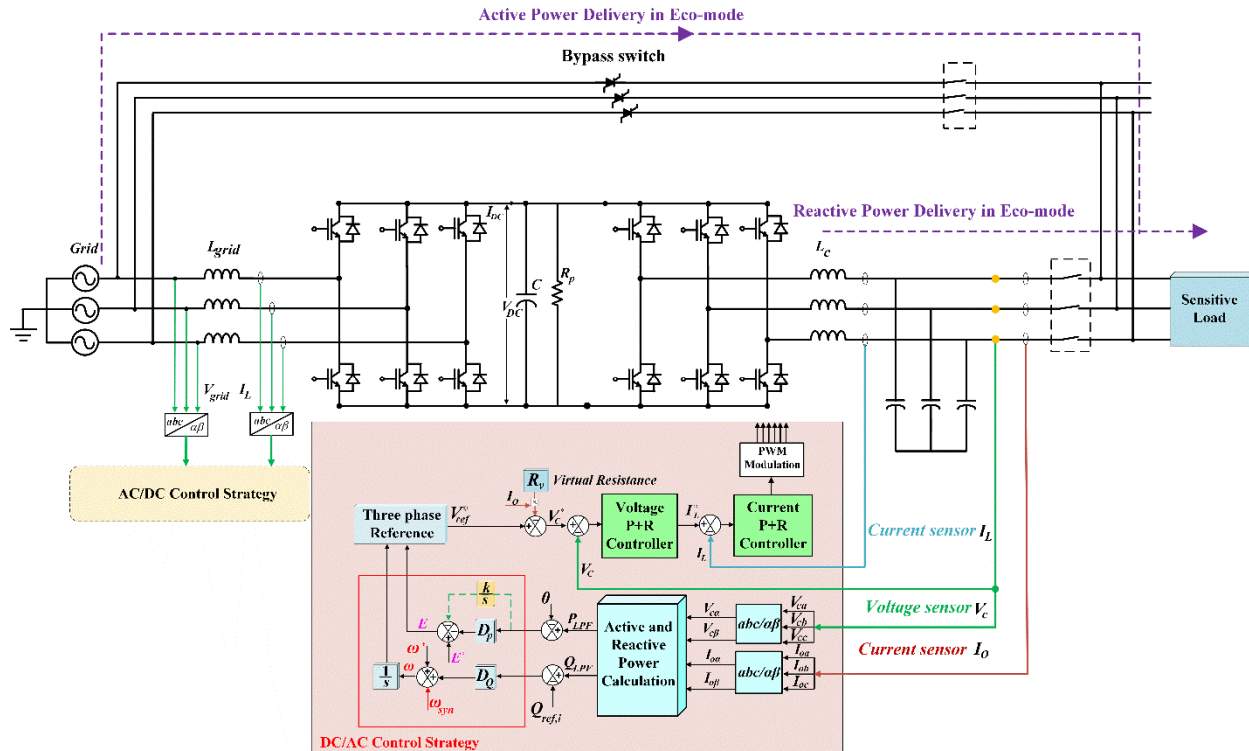Fig.12. The control Strategy of the EEM operation in on-line UPS system.

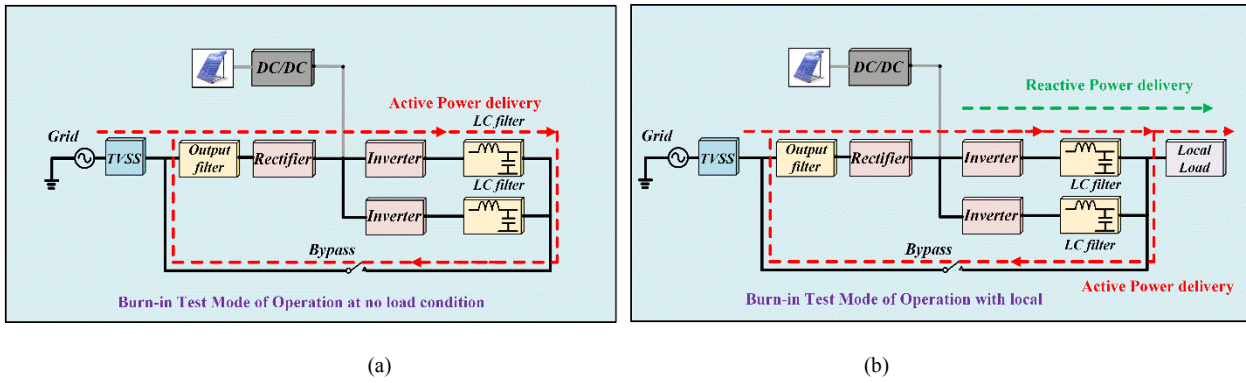(a)   (b)

Fig.13. The power flow in the BTM operation for the on-line UPS system. (a) no load condition (b) local load condition.

Observe (P&O), Hill Climbing algorithm [40] and fuzzy based method [41] can be applied into the system to extract the maximum power. Moreover, in order to regulate the PV output voltage and prevent PV output overcurrent, the dual-loop PI controller is adopted in the system (Fig.10). It should be pointed out that the complex algorithm of MPPT algorithm is not discussed here as it goes beyond the scope of this paper.

B.   Enhanced Eco-Mode and Seamless Transition

When the PV system is unavailable, the UPS system operating mode may transfer from the TNM to the EEM. The active power of the load in the EEM is directly supplied by the grid and its reactive power is provided by the DC/AC inverter, as shown in Fig. 11. Moreover, the transition between the TNM and the EEM should be seamless. In other words, the UPS output voltage should not have abrupt amplitude or frequency change during the transition.

The proposed control strategy of the EEM operation is shown in Fig. 12, where the integral term $\frac{k}{s}$ is added in the $P{\sim}E$ droop control strategy to achieve the active power tracking without a steady-state error. Hence, by setting the active power reference to be zero, the inverter is forced to deliver no active power. In other words, the active power of the load is fully supplied by the grid. Meanwhile, if multiple inverters cooperatively provide the reactive power to the load, the reactive power reference of the droop control strategy in each inverter should be $Q_{ref,i} = \frac{1}{N} Q_{Load}$. So, the droop control strategy in the EEM is expressed as:

$$E = E^* + D_p(P_{LPF} - 0) + \frac{k}{s}(P_{LPF} - 0) \tag{28}$$

$$\omega = \omega^* - D_Q(Q_{LPF} - Q_{ref,i}) + \omega_{syc} \tag{29}$$
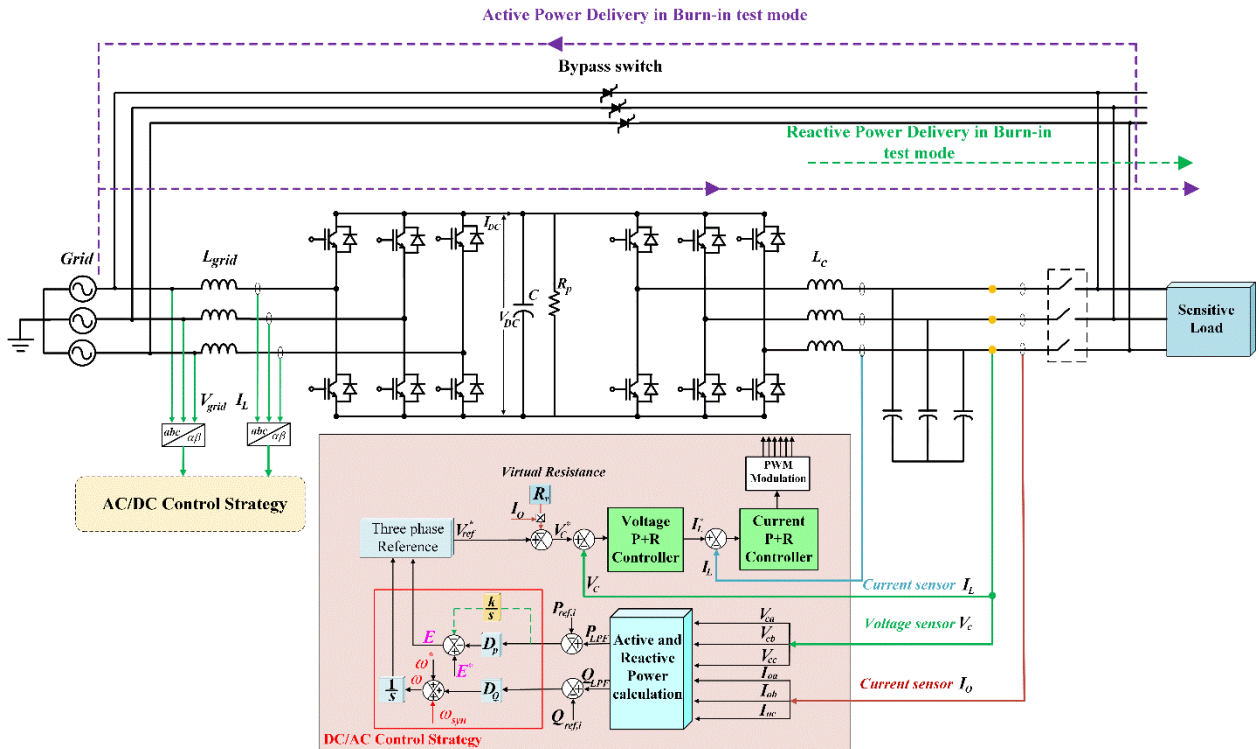

Fig.14. The control Strategy of the BTM operation in operation in the on-line UPS system.

By the comparison of Eq.(21-22) and Eq.(28-29), it is easy to observe that when the gain k and $Q_{ref,i}$ are both set to be zero, the EEM operation returns to the TNM operation. Therefore, the seamless transition can be realized by setting the desired value of the parameter k and $Q_{ref,i}$. Notice that the synchronization term ω_{syc} is added in (29), as all the DC/AC inverters should synchronize with the grid before bypass switch close. In this paper, the synchronization method proposed in [42] is applied for voltage and phase synchronization. Finally, it must be emphasized that the grid fault detection methods [43-45] should be applied in the system to protect it against grid faults. And the EEM has to be switched to the back-up mode in case of grid fault. As this topic is out of the scope of this paper, the details will not be illustrated.

C. Burn-in Test Mode and Seamless Transition

The power flow of the BTM is shown in Fig. 13. Specifically, at no load condition (see Fig.13 (a)), the active power drawn from the grid is fed back again through the bypass switch. On the contrary, when the local load is connected to the UPS system, the power flow is shown in Fig. 13(b), where the active power drawn from the grid flows to the local load and delivers back to the grid, respectively.

The proposed control strategy of the BTM operation is depicted in Fig. 14. Notice that the control strategy is very similar to that of the EEM. The expresison of the droop control strategy in this mode is shown as:

$$E = E^* + D_p\left(P_{LPF} - P_{ref,i}\right) + \frac{k}{s}\left(P_{LPF} - P_{ref,i}\right) \quad (30)$$

$$\omega = \omega^* - D_Q\left(Q_{LPF} - Q_{ref,i}\right) + \omega_{syc} \quad (31)$$

where $P_{ref,i}$ and $Q_{ref,i}$ are the reference active and reactive power, respectively. The integral term $\frac{k}{s}$ forces the output active power to follow the reference one; meanwhile, the reactive power reference for each inverter and is determined by calculating the load reactive power and have the relationship $Q_{ref,i} = \frac{1}{N}Q_{Load}$. It is pointed out that at no load condition, reactive power reference should be set to zero ($Q_{ref,i} = 0$). From the discussion above, the BTM can be easily realized by changing the reference of droop control from the TNM as well. In this way, the seamless transfer among different mode can be realized without affecting the output voltage of the UPS system.

D. Small-Signal Modeling and Analysis

From the discussions of the Section III.B and III.C, it is observed that the EEM and the BTM can be achieved with the same control strategy by adjusting the different reference value. Therefore, in this section, the system small-signal stability of the EEM and the BTM operation is investigated. First, the power flow of the UPS system through a general line impedance is obtained as [46]:

$$P = \left(\frac{EV}{Z}\cos(\varphi) - \frac{V^2}{Z}\right)\cdot\cos(\theta) + \frac{EV}{Z}\sin(\varphi)\sin(\theta) \quad (32)$$

$$Q = \left(\frac{EV}{Z}\cos(\varphi) - \frac{V^2}{Z}\right)\cdot\sin(\theta) - \frac{EV}{Z}\sin(\varphi)\cos(\theta) \quad (33)$$

where P and Q are the instantaneous active and reactive

power of the UPS system that flows out of the general line impedance. E and V are the amplitudes of the inverter output voltage and the common bus voltage, respectively, and φ is the power angle. Z and θ are the magnitude and phase of the output impedance.

Considering that the line impedance most often demonstrate a resistive characteristic in the UPS applications, the power flow of the UPS system can be expressed as:

$$P = \frac{V}{R}(E\cos(\varphi) - V) \cong \frac{V}{R}(E - V) \quad (34)$$

$$Q = -\frac{EV}{R}\sin(\varphi) \cong -\frac{EV}{R}\varphi \quad (35)$$

Accordingly, the active and reactive power variation according to the UPS voltage amplitude and phase angle disturbance can be obtained by:

$$\Delta P = \left(\frac{\partial P}{\partial E}\right)\Delta E + \left(\frac{\partial P}{\partial\varphi}\right)\Delta\varphi = k_{PE}\Delta E + k_{P\varphi}\Delta\varphi \quad (36)$$

$$\Delta Q = \left(\frac{\partial Q}{\partial E}\right)\Delta E + \left(\frac{\partial Q}{\partial\varphi}\right)\Delta\varphi = k_{QE}\Delta E + k_{Q\varphi}\Delta\varphi \quad (37)$$

where the operator Δ indicates a small-signal perturbation around the UPS's operating equilibrium point.

When there are some power fluctuation during the EEM or the BTM, expanding the proposed control strategy in (28)-(29) or (30)-(31) results in the small signal responses of the UPS voltage, which are expressed as:

$$\Delta E = -D_P\Delta P_{LPF} - \frac{k}{s}\Delta P_{LPF} \quad (38)$$

$$\Delta\omega = D_Q\Delta Q_{LPF} \quad (39)$$

$$\Delta P_{LPF} = \frac{1}{\tau s+1}\Delta P \quad (40)$$

$$\Delta Q_{LPF} = \frac{1}{\tau s+1}\Delta Q \quad (41)$$

where τ is the time constant of the low-pass filter in the active and reactive power calculation.

Considering that $\Delta\theta = \frac{1}{s}\cdot\Delta\omega$, and by the simple manipulation of (36)-(37), the dynamic performance of the UPS system in the EEM or BTM operation yields the following expression:

$$(M_{2\times2} - N_{2\times2}\cdot L_{2\times2})\cdot[\Delta E;\ \Delta\varphi]^T = 0 \quad (42)$$

where $M_{2\times2} = \begin{bmatrix} s(\tau s + 1) & 0 \\ 0 & s(\tau s + 1) \end{bmatrix}$, $N_{2\times2} =$

$\begin{bmatrix} -(D_P s + k) & 0 \\ 0 & D_Q \end{bmatrix}$, $L_{2\times2} = \begin{bmatrix} k_{PE} & k_{P\varphi} \\ k_{QE} & k_{Q\varphi} \end{bmatrix}$

The eigenvalues of (42) show the small-signal response of the UPS system during EEM and BTM. In addition, notice that when $k=0$, the matrix $N_{2\times2}$ is expressed as:

$$N_{2\times2} = \begin{bmatrix} -D_P s & 0 \\ 0 & D_Q \end{bmatrix} \quad (43)$$

the corresponding matrix of (43) indicates the behaviour of the UPS system in TNM and PNM operation.

The performance of the system with the different value of the parameter k is evaluated and shown in Fig.15. With UPS system parameters listed in the Table I, Fig.15 shows the root locus of the proposed control strategy, where the droop control

coefficient is fixed while the parameter k varies from 0.0033 to 0.0213. As illustrated, it is a fourth-order system and dynamic performance is mainly determined by the dominant poles of λ_1 and λ_4. It can be observed that when k is increased from 0.0033 to 0.0213, the system stability is improved but has a underdamping response. Therefore, the selection of parameter k involves a tradeoff between the system stability and damping response. In order to obtain the satisfied system damping and stability performance, the parameter k is selected as 0.007.
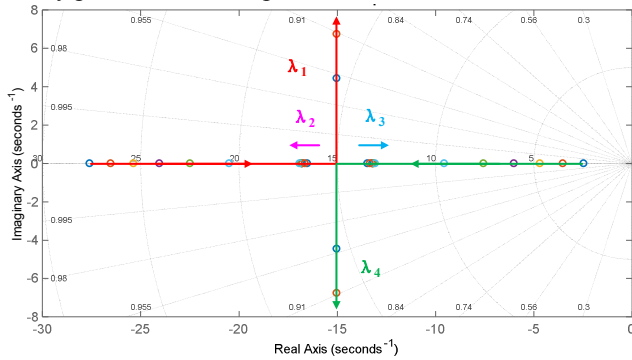

Fig.15. Root Locus with the proposed control strategy when the parameter changes: $0.0033 < k < 0.0213$

IV.   EXPERIMENTAL RESULTS

In order to validate the feasibility of the proposed DC-link voltage control strategy and multi-mode operation of the on-line UPS system, the system diagram shown in Fig.10 is built up and shown in Fig.16. The setup consists of an AC/DC converter, a DC/AC inverter, PV unit and the bypass switch. The DC bus is formed by the DC-link capacitors.

The control algorithm is implemented in dSPACE 1006 platform for real-time control. System parameters are listed in Table I. Waveforms are captured by the oscilloscope.

TABLE I.   SYSTEM AND CONTROLLER PARAMETERS

System Parameters	
Filter Inductor L_f	$1.8mH$
Normal DC link Capacitor	$0.011F$
Sampling frequency f_s	10kHz
Switching loss R_p	1000Ω
DC load	230Ω
Electrical Parameter of the AC/DC and DC/AC Converter	
Converter Rating	1kVA
Phase-to-phase RMS Voltage	208V
Peak phase current	4.4A
DC link voltage	500V
DC-link Voltage Control and Current Control Parameters	
λ_1 of set-point controller	$\dfrac{1}{20}$
λ_2 of disturbance rejection controller	$\dfrac{1}{200}$
k_p of the controller $C_2(s)$	0.2
Current controller k_{pc}	7
Current controller k_{rc}	420
DC-link Voltage Control Comparative Study Parameters	
Proportional Controller	0.02
Integral Controller	0.1
Droop Coefficient	
Frequency droop D_q	0.0001
Voltage droop D_p	0.00005

Integral term k	0.007
Voltage Control Parameter	
Proportional gain k_{pv}	0.2
Resonant gain K_{iv}	100
Current controller Parameter	
Proportional gain K_{pi}	7
Resonant gain K_{ii}	500

A. DC-link Voltage Control Strategy.

First, the effectiveness of the proposed IMC-based DC-link voltage control strategy is verified by using the AC/DC converter of the setup in Fig.16. The PR controller is employed for inner loop current tracking while the two-port IMC-based DC-link voltage controller is implemented for the DC-link voltage regulation (see Fig.4). To further highlight the effectiveness of the proposed method, experimental comparisons are conducted among the traditional PI-based DC-link voltage controller, standard IMC-based control strategy, and the proposed IMC-based DC-link voltage controller with the same closed-loop bandwidth [10]. In the experiment, the DC-link voltage reference is set to be 500 V. A 230Ω resistive load is connected to the DC link to examine the controller's performance from no load to full load condition. This load is suddenly connected to the DC link to examine the controller's disturbance rejection ability. In addition, to emulate the variation of the DC-link capacitance, a different value of capacitance (0.0022F) is considered as the equivalent capacitance change as well.
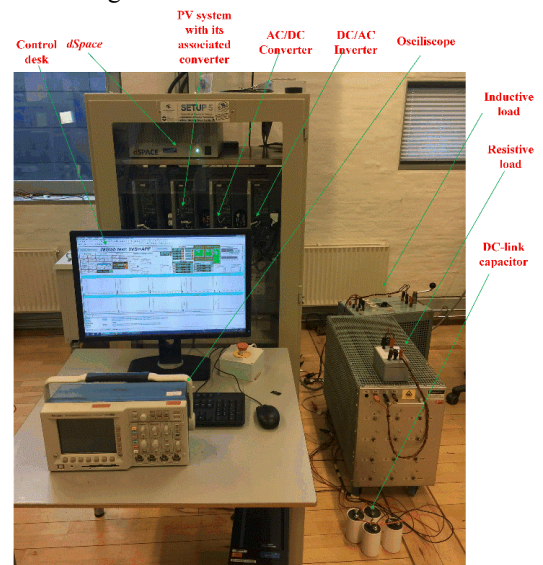
Fig.16. Configuration of the setup

First, the DC-link capacitance is 0.0011 F; the disturbance is generated by disconnecting a 230Ω resistor from the DC link, the DC-link voltage performance under the PI control strategy, standard IMC control strategy and the proposed IMC control strategy are compared in Fig.17 and summarized in Table II. Specifically, it is observed that with PI control strategy, the voltage drop is 60V with 1s of recovery time. By applying standard IMC control strategy to the DC-link voltage regulation,

Fig.17. The performance of PI controller and standard IMC control strategy and proposed IMC control strategy under load disturbance.
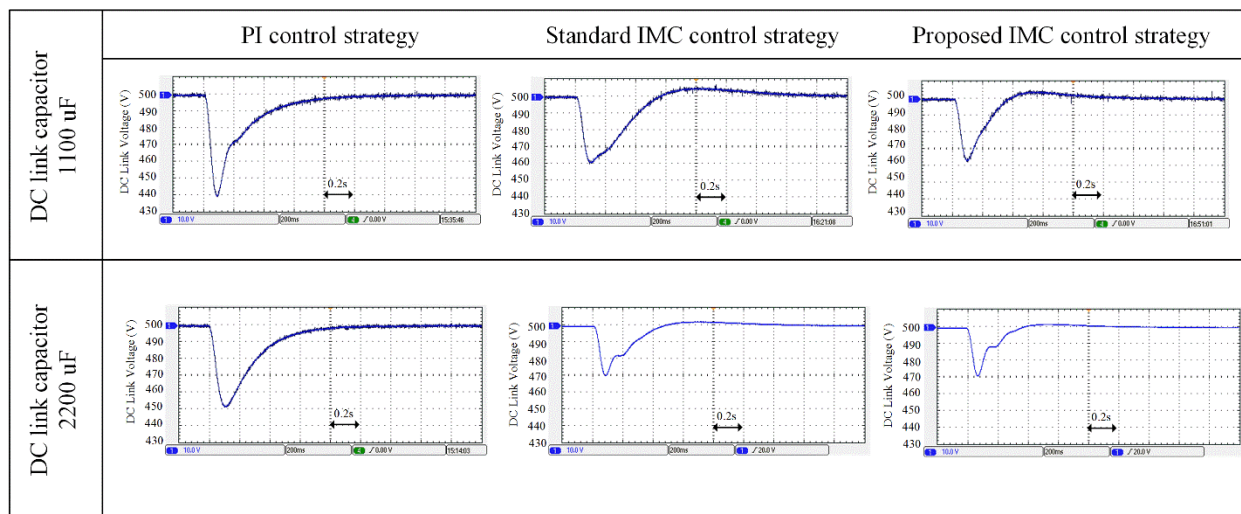
the voltage drop has reduced to 40 V with almost the same recovery time. On the contrary, when the proposed two port IMC based control strategy is applied in the DC-link voltage regulation, the voltage drop reduced to 37V with 0.6s recovery time. Then, the DC-link capacitance has changed to 0.0022F to emulate the DC-link capacitance variation. By employing the PI control strategy, the voltage drop on the DC link is 50V with 0.8s recovery time with. Meanwhile, when the standard IMC control strategy is applied to the DC-link regulation, the voltage drop reduced to 30V with the recovery time of 0.6s. Finally, when the proposed control strategy is implemented in the DC-link, the voltage drop is the same as that with Standard IMC control strategy but the recovery time has shortened to 0.4s.

Overall, compared with the other two methods, the proposed two port IMC based control strategy can significantly reduce the voltage drop and reduce the recovery time under the disturbance.

TABLE II. COMPARISON AMONG THE DIFFERENT CONTROL STRATEGY IN RESPONSE TO THE LOAD STEP

Method	Voltage drop	Recovery time
PI control strategy (1100uF)	60 V	1 s
Standard IMC (1100uF)	40 V	1s
Proposed IMC (1100uF)	37V	0.6s
PI control strategy (2200uF)	50 V	0.8 s
Standard IMC (2200uF)	30 V	0.6s
Proposed IMC (2200uF)	30V	0.4s

B. *Multi-Mode Operation of the on-line UPS system.*

1) *Transition between TNM and PNM operation of the on-line UPS system*

In this section, the schematic diagram with the proposed control strategy in Fig.10 is tested with the setup in Fig.16. Fig.18 shows the active and reactive power waveforms between the TNM and the PNM operation. As can be observed in Fig.18, the load active and reactive power are respectively P_{load}=700W and Q_{load} =120Var. At the TNM operation, the active power delivered from the grid is $P_{in} = 800W$ (blue waveform). Notice that the difference between P_{in} and P_{load} is

caused by the power loss in the UPS system. When the operation mode shifts to the PNM from TNM, the PV output active power is 250W (cyan waveform), so the active power delivery from the grid drops to the 550W. When the PV is unavailable, the operation of UPS system return to the TNM again, and the active power delivery from the grid increases to 800W again, as shown in Fig.18. Meanwhile, it is observed that the load active power and reactive power (green waveform and purple waveform) does not change during the transition. Finally, the load voltage waveform during the transition is shown in Fig.19, where the load voltage is uninterruptible during the transition.
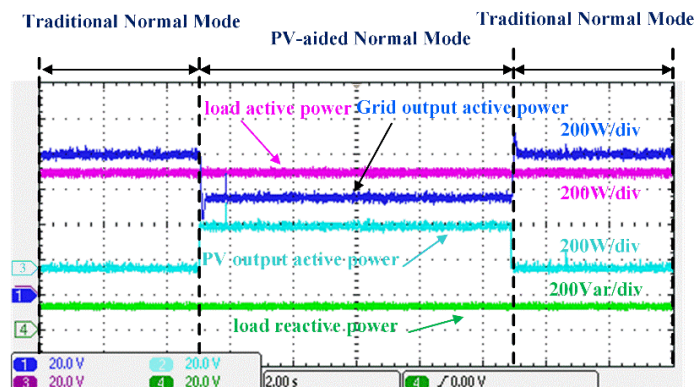

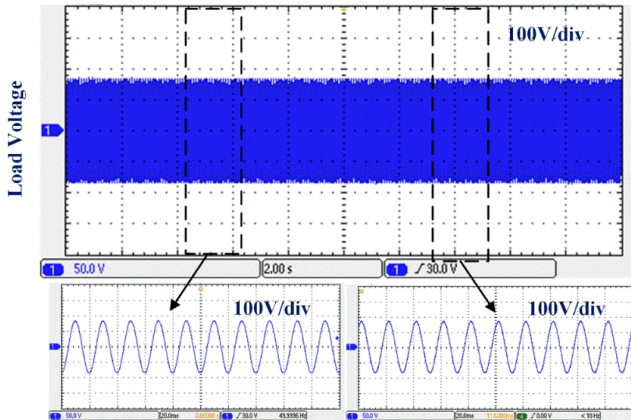Fig.18. Active and reactive power in transfer between TNM and PNM operation.

Fig.19. Load voltage in transfer between between TNM and PNM operation

2) Transition between TNM and EEM operation of the on-line UPS system

In this test, the seamless transition between the TNM and the EEM is evaluated. As shown in Fig. 20(a), when the operation mode of the UPS shifts from TNM to EEM, the load active power provided by the inverter drops to zero (blue waveform), and the 520W of active power is directly provided by the grid through the bypass switch (purple waveform). Meanwhile, the reactive power is still powered by the inverter (cyan waveform). On the contrary, when the operation mode of the UPS shifts from the EEM to the TNM, the load active power is delivered from the inverter and the active power goes through the bypass switch decreased to zero. Fig.20 (b) and (c) shows the load voltage waveforms during the transition, it is indicated that the load voltage is uninterruptible and the whole transition is seamless.
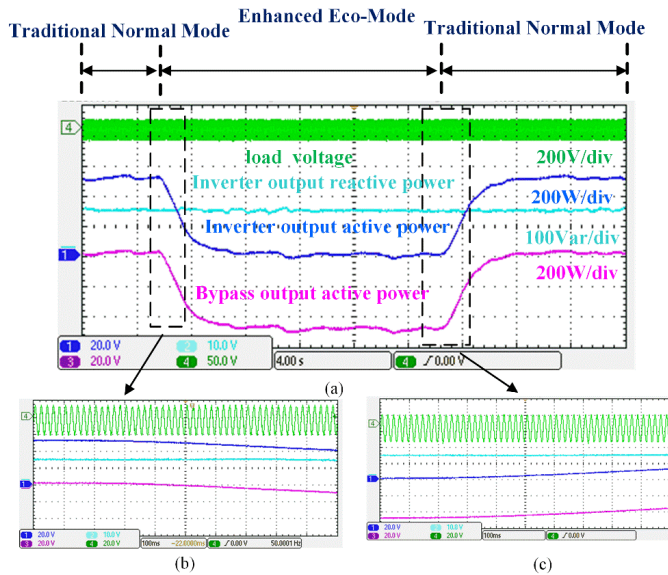

Fig.20. Waveform of transition between the traditional normal mode and the Enhanced Eco-mode.(a) overall waveform (b) Zoomed-in waveform from traditional normal mode to the Enhanced Eco-mode.(c)Zoomed-in waveform from Enhanced Eco-mode to the traditional normal mode.

3) Transition between the traditional normal mode and the Burn-in test mode of the on-line UPS system

(a)Case:1 No Load Condition.

At no load condition, when the UPS system transfer its working mode from the normal mode to the burn-in test mode,

the energy drawn by the inverter should feed back into the grid. In case 1, the output active power of the inverter is set to be 500W (blue waveform), as no load is connected with the UPS system, the 500W of output active power is fed back into the grid through the bypass switch (Fig.21 (a)). Meanwhile, the load voltage during the transition is shown in Fig.21 (b) and (c), where it is observed that the seamless transition is realized as the output voltage has no abrupt change in voltage amplitude and frequency.
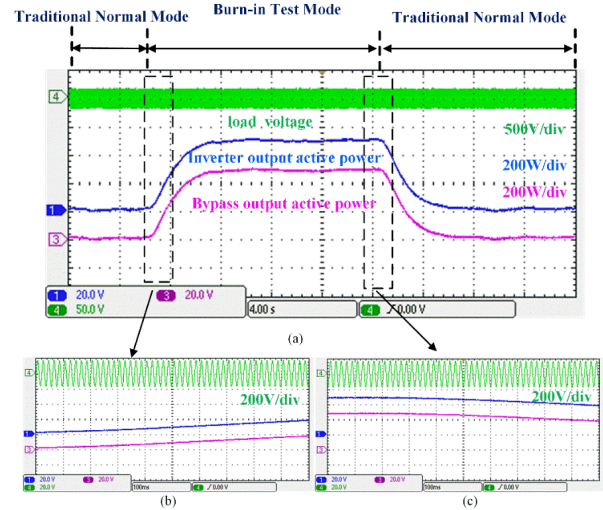

Fig.21. Waveform of transition between the traditional normal mode and the Burn-in test mode at no load condition.(a) overall waveform (b) Zoomed-in waveform from traditional normal mode to the Burn-in test mode.(c) Zoomed-in waveform from the Burn-in test mode to the traditional normal mode.

(b) Case:2   R-L Load is connected during the transition

When the R-L load with 550W of active power and 120Var of reactive power connecting at the UPS system, as can be seen in Fig.22 that the inverter provides the load power. when the UPS system transfer its working mode from TNM to BTM, the active power drawn by the inverter is set to be 850W (blue waveform), the extra 300W of output active power is fed back into the grid through the bypass switch (Fig.22 (a) purple waveform). Meanwhile, the load voltage during the transition is shown in Fig.22 (b) and (c), where it is observed that the seamless transition is realized as the output voltage has no abrupt change in voltage amplitude and frequency.

mode.(c)Zoomed-in waveform from Enhanced Eco-mode to the traditional normal mode.

V. CONCLUSION

In this paper, the multi-modes of operation for the on-line UPS system is proposed. First, the sensor-less IMC based DC-link voltage control strategy has been presented to provide a robust power delivery in the multi-modes of operation. Second, some control strategies for PV-aided normal mode, Enhanced Eco-mode and the Burn-in test mode are respectively presented to achieve the seamless transition in different modes of operation. With the application of these three mode, the cost charged from the grid can be greatly reduced. In addition, these modes of operation can be easily achieved by adjusting the reference value of the inverter in the on-line UPS system. The experimental results showed the effectiveness of the proposed control strategies.
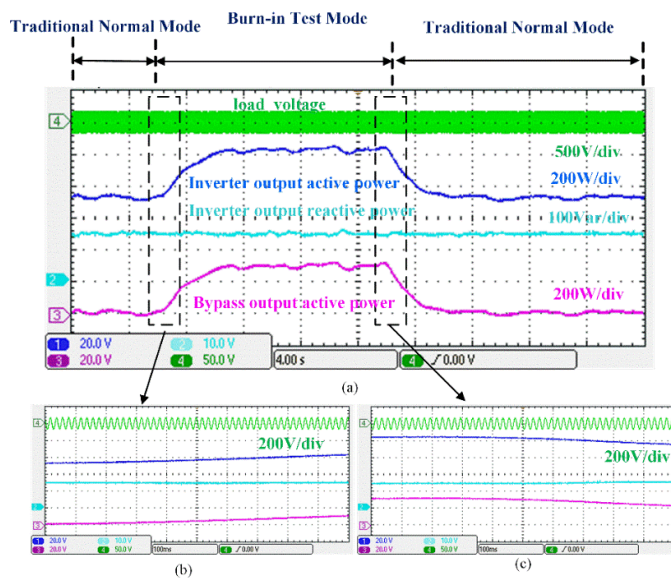
Fig.22. Waveform of transition between the traditional normal mode and the Burn-in test mode at R-L load condition.(a) overall waveform (b) Zoomed-in waveform from traditional normal mode to the Enhanced Eco-

REFERENCES

[1] M. S. Racine, J. D. Parham, and M. H. Rashid, "An overview of uninterruptible power supplies," in *Proceedings of the 37th Annual North American Power Symposium, 2005.*, 2005, pp. 159-164.

[2] G. N. Rajani, "Emerging trends in Uninterrupted Power Supplies: Patents view," in *2016 Biennial International Conference on Power and Energy Systems: Towards Sustainable Energy (PESTSE)*, 2016, pp. 1-5.

[3] "IEC_62040-3-2011 Uninterruptible power systems (UPS) –Part 3: Method of specifying the performance and test requirements."

[4] E. K. Sato, M. Kinoshita, Y. Yamamoto, and T. Amboh, "Redundant High-Density High-Efficiency Double-Conversion Uninterruptible Power System," *IEEE Transactions on Industry Applications,* vol. 46, no. 4, pp. 1525-1533, 2010.

[5] C. Zhang, J. M. Guerrero, J. C. Vasquez, and E. A. A. Coelho, "Control Architecture for Parallel-Connected Inverters in Uninterruptible Power Systems," *IEEE Transactions on Power Electronics,* vol. 31, no. 7, pp. 5176-5188, 2016.

[6] K. Shi, H. Li, C. Hu, and D. Xu, "Topology of super uninterruptible power supply with multiple energy sources," in *2015 9th International Conference on Power Electronics and ECCE Asia (ICPE-ECCE Asia)*, 2015, pp. 1742-1749.

[7] D. Dezhi, C. Linglin, L. Haijin, C. Min, and X. Dehong, "Design of hybrid AC-DC-AC topology for Uninterruptible Power Supply," in *2015 IEEE 2nd International Future Energy Electronics Conference (IFEEC)*, 2015, pp. 1-5.

[8] J. Zhou, H. Li, Z. Liu, C. Hu, and D. Xu, "Control strategy of Li-Ion Battery module in Super UPS," in *2014 International Power Electronics and Application Conference and Exposition*, 2014, pp. 1236-1241.

[9] W. Zhang *et al.*, "Seamless Transfer Control Strategy for Fuel Cell Uninterruptible Power Supply System," *IEEE Transactions on Power Electronics,* vol. 28, no. 2, pp. 717-729, 2013.

[10] N. Rasmussen, "Eco-mode:Benefits and Risks of Energy-saving Modes of UPS operation."

[11] M. Rascon, "Active Eco Mode in Single-Phase UPS," *White Paper*.

[12] L. Giuntini, "Active damping control of multi-mode UPS for power quality improvement," in *2015 17th European Conference on Power Electronics and Applications (EPE'15 ECCE-Europe)*, 2015, pp. 1-10.

[13] H. Shyh-Jier and P. Fu-Sheng, "Design and operation of burn-in test system for three-phase uninterruptible power supplies," *IEEE Transactions on Industrial Electronics,* vol. 49, no. 1, pp. 256-263, 2002.

[14] J. F. Chen, C. L. Chu, T. H. Ai, and C. L. Huang, "The burn-in test of three-phase UPS by energy feedback method," in *Power Electronics Specialists Conference, 1993. PESC '93 Record., 24th Annual IEEE*, 1993, pp. 766-771.

[15] C. L. Chu and J. F. Chen, "Self-load bank for UPS testing by circulating current method," *IEE Proceedings - Electric Power Applications,* vol. 141, no. 4, pp. 191-196, 1994.

[16] F. Blaabjerg, R. Teodorescu, M. Liserre, and A. V. Timbus, "Overview of Control and Grid Synchronization for Distributed Power Generation Systems," *Industrial Electronics, IEEE Transactions on,* vol. 53, no. 5, pp. 1398-1409, 2006.

[17] A. Timbus, M. Liserre, R. Teodorescu, P. Rodriguez, and F. Blaabjerg, "Evaluation of Current Controllers for Distributed Power Generation Systems," *Power Electronics, IEEE Transactions on,* vol. 24, no. 3, pp. 654-664, 2009.

[18] R. I. Amirnaser Yazdani, "Voltage-Sourced Converters in Power Systems : Modeling, Control, and Applications," 2010.

[19] M. Davari and Y. A. R. I. Mohamed, "Robust Multi-Objective Control of VSC-Based DC-Voltage Power Port in Hybrid AC/DC Multi-Terminal Micro-Grids," *IEEE Transactions on Smart Grid,* vol. 4, no. 3, pp. 1597-1612, 2013.

[20] M. Davari and Y. A. R. I. Mohamed, "Dynamics and Robust Control of a Grid-Connected VSC in Multiterminal DC Grids Considering the Instantaneous Power of DC- and AC-Side Filters and DC Grid Uncertainty," *IEEE Transactions on Power Electronics,* vol. 31, no. 3, pp. 1942-1958, 2016.

[21] M. Davari and Y. A. R. I. Mohamed, "Variable-Structure-Based Nonlinear Control for the Master VSC in DC-Energy-Pool Multiterminal Grids," *IEEE Transactions on Power Electronics,* vol. 29, no. 11, pp. 6196-6213, 2014.

[22] C. Zhang, J. M. Guerrero, J. C. Vasquez, and C. M. Seniger, "Modular Plug and Play Control Architectures for Three-Phase Inverters in UPS Applications," *IEEE Transactions on Industry Applications,* vol. 52, no. 3, pp. 2405-2414, 2016.

[23] J. Lu *et al.*, "DC-Link Protection and Control in Modular Uninterruptible Power Supply," *IEEE Transactions on Industrial Electronics,* vol. PP, no. 99, pp. 1-1, 2017.

[24] J. Lu, S. Golestan, M. Savaghebi, J. C. Vasquez, J. M. Guerrero, and A. Marzabal, "An Enhanced State Observer for DC-Link Voltage Control of Three-Phase AC/DC Converters," *IEEE Transactions on Power Electronics,* vol. PP, no. 99, pp. 1-1, 2017.

[25] C. Wang, X. Li, L. Guo, and Y. W. Li, "A Nonlinear-Disturbance-Observer-Based DC-Bus Voltage Control for a Hybrid AC/DC Microgrid," *IEEE Transactions on Power Electronics,* vol. 29, no. 11, pp. 6162-6177, 2014.

[26] J. Liu, S. Vazquez, L. Wu, A. Marquez, H. Gao, and L. G. Franquelo, "Extended State Observer-Based Sliding-Mode Control for Three-Phase Power Converters," *IEEE Transactions on Industrial Electronics,* vol. 64, no. 1, pp. 22-31, 2017.

[27] Q. Zhu, Z. Yin, Y. Zhang, J. Niu, Y. Li, and Y. Zhong, "Research on Two-Degree-of-Freedom Internal Model Control Strategy for Induction Motor Based on Immune Algorithm," *IEEE Transactions on Industrial Electronics,* vol. 63, no. 3, pp. 1981-1992, 2016.

[28] T. Kobaku, S. C. Patwardhan, and V. Agarwal, "Experimental Evaluation of Internal Model Control Scheme on a DC–DC Boost Converter Exhibiting Nonminimum Phase Behavior," *IEEE Transactions on Power Electronics,* vol. 32, no. 11, pp. 8880-8891, 2017.

[29] C. Darab and A. Turcu, "Internal model control for MPPT of a solar PV system," in *2017 International Conference on Modern Power Systems (MPS)*, 2017, pp. 1-4.

[30] J. Yang, W. H. Chen, S. Li, L. Guo, and Y. Yan, "Disturbance/Uncertainty Estimation and Attenuation Techniques in PMSM Drives;A Survey," *IEEE Transactions on Industrial Electronics,* vol. PP, no. 99, pp. 1-1, 2016.

[31] X. Sun, Z. Shi, L. Chen, and Z. Yang, "Internal Model Control for a Bearingless Permanent Magnet Synchronous Motor Based on Inverse System Method," *IEEE Transactions on Energy Conversion,* vol. 31, no. 4, pp. 1539-1548, 2016.

[32] W. Tan and C. Fu, "Linear Active Disturbance-Rejection Control: Analysis and Tuning via IMC," *IEEE Transactions on Industrial Electronics,* vol. 63, no. 4, pp. 2350-2359, 2016.

[33] C. Xia, Y. Yan, P. Song, and T. Shi, "Voltage Disturbance Rejection for Matrix Converter-Based PMSM Drive System Using Internal Model Control," *IEEE Transactions on Industrial Electronics,* vol. 59, no. 1, pp. 361-372, 2012.

[34] S. Li and H. Gu, "Fuzzy Adaptive Internal Model Control Schemes for PMSM Speed-Regulation System," *IEEE Transactions on Industrial Informatics,* vol. 8, no. 4, pp. 767-779, 2012.

[35] G. Stephanopoulos and H.-P. Huang, "The 2-port control system," *Chemical Engineering Science,* vol. 41, no. 6, pp. 1611-1630, 1986/01/01/ 1986.

[36] S. F. G. Graham C. Goodwin, Mario E. Salgado, "CONTROL SYSTEM DESIGN," 2000.

[37] L. Harnefors, K. Pietilainen, and L. Gertmar, "Torque-maximizing field-weakening control: design, analysis, and parameter selection," *IEEE Transactions on Industrial Electronics,* vol. 48, no. 1, pp. 161-168, 2001.

[38] S. Kamran, H. Lennart, N. Hans-Peter, N. Staffan, and T. Remus, "Design, Control and Application of Modular Multilevel Converters for HVDC Transmission Systems," Wiley-IEEE Press, 2016, p. 416.

[39] Y. Chen, J. M. Guerrero, Z. Shuai, Z. Chen, L. Zhou, and A. Luo, "Fast Reactive Power Sharing, Circulating Current and Resonance Suppression for Parallel Inverters Using Resistive-Capacitive Output Impedance," *IEEE Transactions on Power Electronics,* vol. 31, no. 8, pp. 5524-5537, 2016.

[40] M. A. G. d. Brito, L. P. Sampaio, G. Luigi, G. A. e. Melo, and C. A. Canesin, "Comparative analysis of MPPT techniques for PV applications," in *2011 International Conference on Clean Electrical Power (ICCEP)*, 2011, pp. 99-104.

[41] F. Khosrojerdi, S. Taheri, and A. M. Cretu, "An adaptive neuro-fuzzy inference system-based MPPT controller for photovoltaic arrays," in *2016 IEEE Electrical Power and Energy Conference (EPEC)*, 2016, pp. 1-6.

[42] J. C. Vasquez, J. M. Guerrero, M. Savaghebi, J. Eloy-Garcia, and R. Teodorescu, "Modeling, Analysis, and Design of Stationary-Reference-Frame Droop-Controlled Parallel Three-Phase Voltage Source Inverters," *Industrial Electronics, IEEE Transactions on,* vol. 60, no. 4, pp. 1271-1280, 2013.

[43] Q. Sun, J. M. Guerrero, T. Jing, J. C. Vasquez, and R. Yang, "An Islanding Detection Method by Using Frequency Positive Feedback Based on FLL for Single-Phase Microgrid," *IEEE Transactions on Smart Grid,* vol. 8, no. 4, pp. 1821-1830, 2017.

[44] S. D. Kermany, M. Joorabian, S. Deilami, and M. A. S. Masoum, "Hybrid Islanding Detection in Microgrid With Multiple Connection Points to Smart Grids Using Fuzzy-Neural Network," *IEEE Transactions on Power Systems,* vol. 32, no. 4, pp. 2640-2651, 2017.

[45] M. Bakhshi, R. Noroozian, and G. B. Gharehpetian, "Novel Islanding Detection Method for Multiple DGs Based on Forced Helmholtz Oscillator," *IEEE Transactions on Smart Grid,* vol. PP, no. 99, pp. 1-1, 2017.

[46] J. M. Guerrero, L. Hang, and J. Uceda, "Control of Distributed Uninterruptible Power Supply Systems," *IEEE Transactions on Industrial Electronics,* vol. 55, no. 8, pp. 2845-2859, 2008.

Jinghang Lu (S'14) received the B.Sc. degree in electrical engineering from Harbin Institute of Technology, China, in 2009, two M.Sc. degrees both in electrical engineering from Harbin Institute of Technology, China, in 2011, and University of Alberta, Canada, in 2014, respectively, and the Ph.D. degree in Power Electronics from Aalborg University, Aalborg, Denmark, in 2018.

He is currently working with Aalborg University, Denmark. His research interests include uninterruptible power supply, microgrid, and control of power converters.

Mehdi Savaghebi (S'06-M'15-SM'15) was born in Karaj, Iran, in 1983. He received the B.Sc. degree from University of Tehran, Iran, in 2004 and the M.Sc. and Ph.D. degrees with highest honors from Iran University of Science and Technology, Tehran, Iran in 2006 and 2012, respectively, all in Electrical Engineering. From 2007 to 2014, he was a Lecturer in Electrical Engineering Department, Karaj Branch, Islamic Azad University. In 2010, he was a visiting Ph.D. Student with the Department of Energy Technology, Aalborg University, Aalborg, Denmark and with the Department of Automatic Control Systems and Computer Engineering, Technical University of Catalonia, Barcelona, Spain.

From 2014 to 2017, he was a Postdoc Fellow in the Department of Energy Technology, Aalborg University where he is currently an Associate Professor. His main research interests include distributed generation systems, microgrids, power quality, Internet of Things (IoT) and smart metering. Dr. Savaghebi has been a Guest Editor of Special Issue on Power Quality in Smart Grids, IEEE Transactions on Smart Grid. He is a member of Technical Committee of Renewable Energy Systems, IEEE Industrial Electronics Society and vice-chair of sub-committee on Smart Buildings, IEEE Power and Energy Society.

Saeed Golestan (M'11-SM'15) received the B.Sc. degree in electrical engineering from Shahid Chamran University of Ahvaz, Iran, in 2006, and the M.Sc. degree in electrical engineering from the Amirkabir University of Technology, Tehran, Iran, in 2009.

He is currently working towards the Ph.D. degree at the Department of

Energy Technology, Aalborg University, Denmark. His research interests include phase-locked loop and nonlinear filtering techniques for power engineering applications, power quality measurement and improvement, estimation of power system parameters, and control of power converters.

Juan C. Vasquez (M'12-SM'14) received the B.S. degree in electronics engineering from the Autonomous University of Manizales, Manizales, Colombia, and the Ph.D. degree in automatic control, robotics, and computer vision from the Technical University of Catalonia, Barcelona, Spain, in 2004 and 2009, respectively. He was with the Autonomous University of Manizales working as a teaching assistant and the Technical University of Catalonia as a Post-Doctoral Assistant in 2005 and 2008 respectively. In 2011, He was Assistant Professor and from 2014 he is working as an Associate Professor at the Department of Energy Technology, Aalborg University, Denmark where He is the Vice Programme Leader of the Microgrids Research Program (see microgrids.et.aau.dk). He was a Visiting Scholar at the Center of Power Electronics Systems (CPES) at Virginia Tech and a visiting professor at Ritsumeikan University, Japan. His current research interests include operation, advanced hierarchical and cooperative control, optimization and energy management applied to distributed generation in AC/DC Microgrids, maritime microgrids, advanced metering infrastructures and the integration of Internet of Things into the SmartGrid. Dr Vasquez is a Associate Editor of IET POWER ELECTRONICS and a Guest Editor of the IEEE TRANSACTIONS ON INDUSTRIAL INFORMATICS Special Issue on Energy Internet. In 2017, Dr. Vasquez was awarded as Highly Cited Researcher by Thomson Reuters. Dr. Vasquez is currently a member of the IEC System Evaluation Group SEG4 on LVDC Distribution and Safety for use in Developed and Developing Economies, the Renewable Energy Systems Technical Committee TC-RES in IEEE Industrial Electronics, PELS, IAS, and PES Societies.

Josep M. Guerrero (S'01-M'04-SM'08-FM'15) received the B.S. degree in telecommunications engineering, the M.S. degree in electronics engineering, and the Ph.D. degree in power electronics from the Technical University of Catalonia, Barcelona, in 1997, 2000 and 2003, respectively. Since 2011, he has been a Full Professor with the Department of Energy Technology, Aalborg University, Denmark, where he is responsible for the Microgrid Research Program (www.microgrids.et.aau.dk). From 2012 he is a guest Professor at the Chinese Academy of Science and the Nanjing University of Aeronautics and Astronautics; from 2014 he is chair Professor in Shandong University; from 2015 he is a distinguished guest Professor in Hunan University; and from 2016 he is a visiting professor fellow at Aston University, UK, and a guest Professor at the Nanjing University of Posts and Telecommunications.

His research interests is oriented to different microgrid aspects, including power electronics, distributed energy-storage systems, hierarchical and cooperative control, energy management systems, smart metering and the internet of things for AC/DC microgrid clusters and islanded minigrids; recently specially focused on maritime microgrids for electrical ships, vessels, ferries and seaports. Prof. Guerrero is an Associate Editor for the IEEE TRANSACTIONS ON POWER ELECTRONICS, the IEEE TRANSACTIONS ON INDUSTRIAL ELECTRONICS, and the IEEE Industrial Electronics Magazine, and an Editor for the IEEE TRANSACTIONS on SMART GRID and IEEE TRANSACTIONS on ENERGY CONVERSION. He has been Guest Editor of the IEEE TRANSACTIONS ON POWER ELECTRONICS Special Issues: Power Electronics for Wind Energy Conversion and Power Electronics for Microgrids; the IEEE TRANSACTIONS ON INDUSTRIAL ELECTRONICS Special Sections: Uninterruptible Power Supplies systems, Renewable Energy Systems, Distributed Generation and Microgrids, and Industrial Applications and Implementation Issues of the Kalman Filter; the IEEE TRANSACTIONS on SMART GRID Special Issues: Smart DC Distribution Systems and Power Quality in Smart Grids; the IEEE TRANSACTIONS on ENERGY CONVERSION Special Issue on Energy Conversion in Next-generation Electric Ships. He was the chair of the Renewable Energy Systems Technical Committee of the IEEE Industrial Electronics Society. He received the best paper award of the IEEE Transactions on Energy Conversion for the period 2014-2015, and the best paper prize of IEEE-PES in 2015. As well, he received the best paper award of the Journal of Power Electronics in 2016. In 2014, 2015, and 2016 he was awarded by Thomson Reuters as Highly Cited Researcher, and in 2015 he was elevated as IEEE Fellow for his contributions on "distributed power systems and microgrids."

Albert Marzàbal received the B.S. degree in telecommunications engineering, the M.S. degree in electronics engineering (with the highest distinction), and the diploma of advanced studies (DEA) in the Ph.D. program of Vision, Control, and Robotics from the Technical University of Catalonia, Barcelona, Catalonia, in 2000, 2005, and 2009, respectively. He now works in the research laboratory of Salicru, S.A., a company that has designed, manufactured and commercialized power electronics products for the key sectors of the energy market since 1965. He had some publications, and worked as a developer at Institut de Robòtica Informàtica Industrial, and as a professor in engineering topics at Technical University of Catalonia for over 10 years.